Giant fluctuations at a granular phase separation threshold

Baruch Meerson,[1] Thorsten Pöschel,[2] Pavel V. Sasorov,[3] and Thomas Schwager[2]

[1]*Racah Institute of Physics, Hebrew University of Jerusalem, Jerusalem 91904, Israel*
[2]*Institut für Biochemie, Charité, Monbijoustrasse 2, 10117 Berlin, Germany*
[3]*Institute of Theoretical and Experimental Physics, Moscow 117218, Russia*

We investigate a phase separation instability that occurs in a system of nearly elastically colliding hard spheres driven by a thermal wall. If the aspect ratio of the confining box exceeds a threshold value, granular hydrostatics predict phase separation: the formation of a high-density region coexisting with a low-density region along the wall that is opposite to the thermal wall. Event-driven molecular dynamics simulations confirm this prediction. The theoretical bifurcation curve agrees with the simulations quantitatively well below and well above the threshold. However, in a wide region of aspect ratios around the threshold, the system is dominated by fluctuations, and the hydrostatic theory breaks down. Two possible scenarios of the origin of the giant fluctuations are discussed.

I. INTRODUCTION

Dynamics of a system of inelastically colliding hard spheres have attracted a great deal of recent interest [1,2], in particular in the context of validity of kinetic theory and hydrodynamics of rapid granular flow developed in the 1980s [3]. Hydrodynamics looks ideally suitable for a description of large-scale patterns observed in rapid granular flows: a plethora of clustering phenomena [4], vortices [5], oscillons [6], shocks [7], etc., that are difficult to understand in the language of individual particles. However, a first-principles derivation of a universally applicable continuum theory of granular gas is not a simple task, even in the dilute limit. The use of the Enskog equation, the starting point of a systematic derivation of the constitutive relations of granular hydrodynamics, is based on the *molecular chaos* hypothesis. This hypothesis is justified for not too large densities and for an ensemble of *elastic* hard spheres. Its use for *inelastic* hard spheres is not obvious, as inelasticity of the particle collisions introduces interparticle correlations [8]. The correlations become stronger as the inelasticity of the collisions increases. On the contrary, for *nearly elastic* collisions, $1 - r^2 \ll 1$ (where r is the coefficient of normal restitution) the correlations are small, and the Enskog equation can be safely used.

An important additional assumption, made in the process of the derivation of hydrodynamics from the Enskog equation, is scale separation. Hydrodynamics demands that the mean free path of the particles be much less than any characteristic length scale, and the mean time between two consecutive collisions be much less than any characteristic time scale described hydrodynamically. This condition should be verified, in every specific system, after the hydrodynamic problem is solved and the characteristic length and time scales determined. Again, it is safe to say that this condition can be satisfied if the particle collisions are nearly elastic [9–11]. Restrictive as it is, the nearly elastic limit is conceptually important just because granular hydrodynamics is expected to work here.

Another potentially important, albeit largely unexplored,

limitation of the validity of granular hydrodynamics (or, rather, of any continuum approach to rapid granular flow) is due to the noise caused by the discrete nature of particles. Noise is stronger here than in classical (molecular) fluids simply because the number of particles is much smaller. In addition, noise can be amplified at thresholds of hydrodynamic instabilities as found, for example, in Rayleigh-Bénard convection of classical fluids [12].

The validity of hydrodynamic description in general, and the accuracy of constitutive relations in particular, can be conveniently checked on symmetry-breaking instabilities that are abundant in rapid granular flows. The example of a symmetry-breaking instability that we consider in this work deals with a very simple setting: a two-dimensional (2D) system of nearly elastically colliding hard spheres, confined by a rectangular box and driven by a thermal sidewall at zero gravity. The setting is described in detail in Sec. II. The basic steady state here is the ''stripe state'': a stripe of enhanced density at the wall opposite to the driving wall [10]. In the continuum language, the stripe state is uniform in the lateral direction, by which we mean the direction parallel to the driving wall. Within a certain range of parameters (delineated below), steady-state equations of granular hydrodynamics predict spontaneous symmetry-breaking instability of the stripe state, when the aspect ratio of the confining box exceeds a certain threshold [13–16]. The instability leads to phase separation: the development of ''droplets'' (high-density domains) coexisting with ''bubbles'' (low-density domains). For *very* large aspect ratios of the box, this symmetry-breaking instability has been recently observed in event-driven molecular dynamics (EMD) simulations, and described by a phenomenological continuum model [17]. The present work is devoted to a more detailed investigation of the phase separation instability in the range of aspect ratios *comparable* to the threshold value. We employ, in Sec. III, the equations of granular hydrodynamics (or rather hydrostatics) to compute the supercritical bifurcation curve for the phase separation instability. Then we report, in Sec. IV, on extensive EMD simulations that show that this bifurcation curve is quantitatively accurate well below and well above

the threshold value of the aspect ratio. Unexpectedly, the hydrostatic theory fails in a relatively *wide* region of aspect ratios around the threshold value, where the system is found to exhibit giant fluctuations. In an attempt to get insight into the mechanism of this anomaly, we investigate, also in Sec. IV, the dependence of the magnitude of fluctuations on the total number of particles in the system. A summary and discussion of our results is presented in Sec. V.

II. MODEL SYSTEM AND HYDROSTATIC EQUATIONS

Let N hard spheres of diameter d and mass $m=1$ move in a 2D rectangular box $L_x \times L_y$. The inelasticity of particle collisions is parametrized by a constant coefficient of normal restitution r. Particle collisions with three of the walls are elastic. The fourth, thermal wall is located at $x = L_x$. Upon collision with it, the normal component of the particle velocity is drawn from a Maxwell distribution with temperature T_0 [10], while the tangential component of the particle velocity is preserved.

Working in the nearly elastic limit $1-r^2 \ll 1$ and employing the Navier-Stokes hydrodynamics [3], we introduce the number density $n(\mathbf{r},t)$, granular temperature $T(\mathbf{r},t)$, and mean-flow velocity $\mathbf{v}(\mathbf{r},t)$. Energy input at the thermal wall can be balanced by the dissipation due to interparticle collisions. Therefore, we assume that the system reaches a zero-mean-flow steady state $\mathbf{v} = \mathbf{0}$, and is therefore describable by the simple momentum and energy balance equations:

$$p = \text{const}, \quad \nabla \cdot (\kappa \nabla T) = I. \qquad (1)$$

Here p is the pressure, κ is the thermal conductivity, and I is the rate of energy loss by collisions. The hydrostatic equations (1) should be supplemented by constitutive relations: p, κ, and I in terms of n and T. These relations are derivable systematically only in the dilute limit [3,18]. Being interested in moderate densities, we shall employ the well-known constitutive relations by Jenkins and Richman [20], which account for excluded particle volume. In the nearly elastic limit one can neglect the inelasticity correction terms in p and κ, as well as the small density gradient term, proportional to $1-r$, in the heat flux [19].

Equations (1) can be rewritten in terms of a single variable: the scaled inverse density $z(x,y) = n_c/n(x,y)$, where $n_c = 2/(\sqrt{3}d^2)$ is the hexagonal close-packing density. In scaled coordinates $\mathbf{r}/L_x \to \mathbf{r}$, the box dimensions become $1 \times \Delta$, where $\Delta = L_y/L_x$ is the box aspect ratio. We obtain [15]

$$\nabla \cdot [F(z)\nabla z] = \eta Q(z), \qquad (2)$$

where $F(z) = A(z)B(z)$,

$$A(z) = \frac{G\left[1 + \frac{9\pi}{16}\left(1 + \frac{2}{3G}\right)^2\right]}{z^{1/2}(1+2G)^{5/2}},$$

$$B(z) = 1 + 2G + \frac{\pi}{\sqrt{3}} \frac{z\left(z + \frac{\pi}{16\sqrt{3}}\right)}{\left(z - \frac{\pi}{2\sqrt{3}}\right)^3},$$

$$Q(z) = \frac{6}{\pi} \frac{z^{1/2}G}{(1+2G)^{3/2}},$$

$$G = G(z) = \frac{\pi}{2\sqrt{3}} \frac{z - \frac{7\pi}{32\sqrt{3}}}{\left(z - \frac{\pi}{2\sqrt{3}}\right)^2}, \qquad (3)$$

and $\eta = (2\pi/3)(1-r)(L_x/d)^2$ is the hydrodynamic inelasticity parameter. Introducing $\psi(x,y) = \int_0^z F(z')dz'$, we arrive at the following equation:

$$\nabla^2 \psi = \eta \tilde{Q}(\psi), \qquad (4)$$

where $\tilde{Q}(\psi) = Q[z(\psi)]$ (in the following the symbol $\sim$ is omitted). The boundary conditions are

$$\frac{\partial \psi}{\partial x}\bigg|_{x=0} = \frac{\partial \psi}{\partial y}\bigg|_{x=1} = \frac{\partial \psi}{\partial y}\bigg|_{y=-\Delta/2} = \frac{\partial \psi}{\partial y}\bigg|_{y=\Delta/2} = 0. \qquad (5)$$

Finally, the number of particles is conserved:

$$\frac{1}{\Delta}\int_{-\Delta/2}^{\Delta/2}\int_0^1 \frac{dxdy}{z(\psi)} = \frac{N}{L_x L_y n_c} \equiv f. \qquad (6)$$

The hydrostatic problem (4)–(6) is fully determined by three scaled parameters: the area fraction f, η, and Δ. Notice that the steady-state *density* distributions are independent of T_0 as the hard-sphere model does not introduce any intrinsic energy scale.

III. STRIPE STATE, SYMMETRY-BREAKING INSTABILITY, AND BIFURCATION CURVE

The trivial steady state of the system is a laterally uniform cluster of particles located at the wall $x=0$, opposite to the thermal wall [10]; see Fig. 1. This state will be called the stripe state. In the language of hydrodynamics, it is described by the y-independent solution of Eqs. (4)–(6); we shall denote it by $z = Z(x)$, correspondingly $\psi = \Psi(x)$.

It was predicted that, in a wide region of the parameter space (f,η,Δ), the stripe state should give way, by a symmetry-breaking bifurcation (either supercritical or subcritical), to a laterally asymmetric state [13–16]. For very large aspect ratios Δ, this phase separation instability has been observed in EMD simulations [17]. For a laterally asymmetric steady state one can write

$$\psi(x,y) = \Psi(x) + \sum_n \varphi_n(x)\exp(inky), \qquad (7)$$
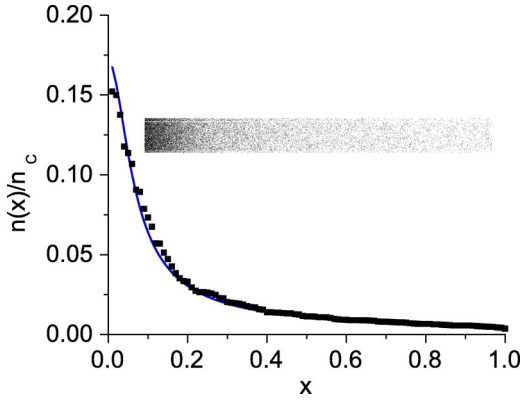
FIG. 1. The stripe state for $\eta = 11\,050$ and $f = 0.025$. We show the scaled density vs scaled coordinate x obtained (a) by solving numerically Eqs. (4)–(6) in one dimension (line) and (b) in EMD simulation with $N = 2 \times 10^4$ particles for $\Delta = 0.1$ (squares). The inset shows a snapshot of the system from the EMD simulation (the hot wall is on the right). Because of a finite image resolution the particle number density in this and other snapshots may look higher than it is.

where $\varphi_{-n}(x) = \varphi_n^*(x)$. What happens close to the supercritical bifurcation point? Here the leading terms are those with $n = \pm 1$, while $\varphi_0 \sim \varphi_1^2$, $\varphi_2 \sim \varphi_1^2$, $\varphi_3 \sim \varphi_1^3$, etc. The bifurcation point itself can be found from the linear eigenvalue problem

$$\varphi_{1k}'' - \eta Q_\Psi \varphi_{1k} - k_c^2 \varphi_{1k} = 0, \qquad (8)$$

$$\varphi_{1k}'(0) = 0 \quad \text{and} \quad \varphi_{1k}(1) = 0, \qquad (9)$$

which was analyzed in Refs. [13–15]. Here

$$Q_\Psi(x) = F^{-1} dQ/dz|_{z=Z(x)}.$$

For given η and f, one obtains the eigenvalue $k = k_c(\eta, f)$ and corresponding eigenfunction $\varphi_{1k}(x)$. The modes with $k < k_c(\eta, f)$ are unstable. Within a spinodal interval $f_1(\eta) < f < f_2(\eta)$, the effective lateral compressibility of the gas is *negative*, and this is the mechanism of the instability [15,17]. At $\eta \gg 1$, there is a range of f such that k_c and $\varphi_{1k}(x)$ become insensitive to the precise form of the boundary conditions at the driving wall. This is the universal "localization regime," when the eigenfunction $\varphi_{1k}(x)$ is exponentially localized at the wall opposite to the driving wall [13,15]. The spinodal interval exists for $\eta_c < \eta < \infty$; it shrinks to zero at $\eta = \eta_c \simeq 344.3$ [17,21]. It has been recently shown, for a different boundary condition at the driving wall, that the bifurcation from the stripe state to a phase separated state is supercritical within some density interval $f_-(\eta) < f < f_+(\eta)$, which is located within the spinodal interval. On each of the intervals $f_1 < f < f_-$ and $f_+ < f < f_2$, the bifurcation is subcritical [16].

As we have already noted, the present work focuses on the phase separation via a supercritical bifurcation. To obtain the asymptotics of the supercritical bifurcation curve close to onset, one should go to the second order of the perturbation theory and take into account, in Eq. (7), the terms $n = 0$,

± 1, and ± 2. In this way one obtains three linear ordinary differential equations, presented in Ref. [16], where the same problem was solved for a different boundary condition at the driving wall. The solvability condition for these equations [22] yields the bifurcation curve: A versus $k_c^2 - k^2$. The amplitude A can be uniquely defined by the relation

$$\varphi(x) = A\Phi_0(x) + A|A|^2 \delta\varphi(x),$$

where $\Phi_0(x)$ is the solution of Eqs. (8) and (9) such that $\Phi_0(0) = 1$, while $\delta\varphi(x) = O(1)$. This yields

$$A(k_c^2 - k^2) = CA|A|^2,$$

where $C = \text{const}$. The trivial solution $A = 0$ describes the stripe state, while the nontrivial one, $k_c^2 - k^2 = C|A|^2$, describes the bifurcated state. The constant C can be computed numerically. $C > 0(<0)$ corresponds to supercritical (subcritical) bifurcation. We present here the resulting bifurcation curve for Y_c, the (normalized) y coordinate of the center of mass of the granulate,

$$Y_c = \frac{\int_0^1 dx \int_{-\Delta/2}^{\Delta/2} y n(x,y) dy}{\Delta \int_0^1 dx \int_{-\Delta/2}^{\Delta/2} n(x,y) dy}. \qquad (10)$$

Let us fix η and f and treat Δ as the control parameter. When Δ is slightly larger than $\Delta_c = \pi/k_c(f)$, only the fundamental mode $k = \pi/\Delta$ is unstable, and the bifurcation curve has the form

$$|Y_c| = \Upsilon(\Delta - \Delta_c)^{1/2}. \qquad (11)$$

Here

$$\Upsilon = \frac{2^{3/2} f_0}{C^{1/2} \Delta_c f} \quad f_0 = 2 \int_0^1 dx \frac{\Phi_{01}}{Z^2 F},$$

and $\Phi_{01}(x)$ is the solution of initial-value problem for Eq. (8) with the initial conditions $Y(0) = 1$ and $Y'(0) = 0$. Equation (11) assumes $C > 0$: a supercritical bifurcation. We have found that, at fixed η, $C > 0$ on an interval $f_-(\eta) < f < f_+(\eta)$ that lies within the spinodal interval (f_1, f_2). On the intervals $f_1 < f < f_-$ and $f_+ < f < f_2$ the coefficient C becomes negative which indicates a subcritical bifurcation. The solid line in Fig. 6 shows the supercritical bifurcation curve (11) for $\eta = 11\,050$ and $f = 0.025$. Here $\Delta_c \simeq 0.514$ and $\Upsilon \simeq 0.142$.

When Δ is well above Δ_c, the weakly nonlinear theory is invalid, and a numerical solution of the fully nonlinear hydrostatic problem (4)–(6) is needed for the determination of $|Y_c|$. An alternative approach is a hydrodynamic simulation that is a numerical solution of the hydrodynamic equations. Numerical simulations of this type were done in Ref. [16] for a different version of constitutive relations [10] and a different boundary condition at the driving wall. It was observed that the phase separation instability produces multiple clusters whose further dynamics proceed as gas-mediated com-
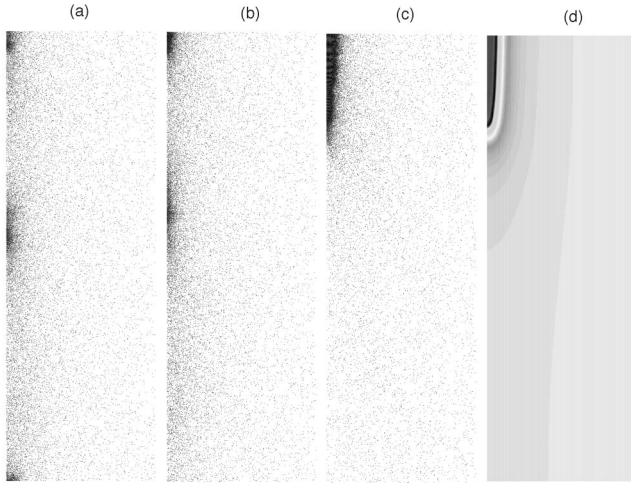
FIG. 2. Nucleation and coarsening of clusters as observed in an EMD simulation with $N = 2 \times 10^4$ particles for $\eta = 11\,050$, $f = 0.025$, and $\Delta = 3$. The hot wall is on the right. The scaled times are 14 425 (a), 26 218 (b) and 191 616 (c). Panel (d) is a density map of the steady state obtained by Livne in a simplified hydrodynamic simulation for the same hydrodynamic parameters [23].

petition and coarsening. Direct merging of clusters can also occur. The final symmetry-broken state, as observed in the hydrodynamic simulations, is always a single, almost densely packed stationary 2D cluster coexisting with gas (or dilute bubble coexisting with denser fluid). The cluster is located in one of the system's corners (unless periodic boundary conditions are used). This scenario was confirmed in a hydrodynamic simulation of the *present* system (for $\eta = 11\,050$, $f = 0.025$, and $\Delta = 3$) done by Livne [23]. A density map of the hydrodynamic final state in this case is shown in Fig. 2(d). The steady-state value $|Y_c| \simeq 0.265$, obtained in this simulation, is shown by the circle in Fig. 6.

IV. EMD SIMULATIONS

A. Simulation method, parameters, and diagnostics

We put the predictions of the granular hydrostatics into test by doing extensive EMD simulations of this system. Most of the simulations were done with $N = 2 \times 10^4$ particles: hard disks of diameter $d = 1$ and mass $m = 1$. The thermal wall temperature is $T_0 = 1$, so the scaled time unit is $d(m/T_0)^{1/2} = 1$. A standard event-driven algorithm [24] was used. Two of the hydrodynamic parameters, $\eta = 11\,050$ and $f = 0.025$, were fixed in all simulations, while Δ was varied in the range of $0.1 < \Delta < 3$. This was achieved by varying L_x, L_y, and r. Indeed, for a fixed η, f, Δ, and N the coefficient of normal restitution

$$r = 1 - \frac{\sqrt{3}\,\eta f \Delta}{\pi N} \qquad (12)$$

and the system's dimensions

$$L_x = \left(\frac{\sqrt{3}N}{2f\Delta} \right)^{1/2} \quad \text{and} \quad L_y = \left(\frac{\sqrt{3}N\Delta}{2f} \right)^{1/2} \qquad (13)$$

are uniquely determined. For the values of the parameters that we used, r was always in the range of nearly elastic collisions: $r \geqslant 0.977$. The initial spatial distribution of the particles was (statistically) uniform, while the initial velocity distribution was Maxwell's with the wall temperature $T_0 = 1$. The center-of-mass coordinate $Y_c(t)$ was used as a quantitative probe of the lateral asymmetry of the system. Before taking the steady-state measurements we waited until transients died out. This was monitored by the time dependence of the average kinetic energy of the particles (which first decayed and then approached an almost constant value) and by the time dependence of the center of mass itself, see below. Selected movies of these simulations can be downloaded from Ref. [37].

B. Final states at different Δ

The EMD simulations showed that, at aspect ratios *well below* the threshold value of $\Delta = \Delta_c \simeq 0.514$, the final state is a (weakly fluctuating) stripe state. The number density profile versus x, found in the simulations, compares very well with the hydrostatic solution (see Fig. 1), while $Y_c(t)$ stays close to zero. Notice that the Jenkins-Richman constitutive relations [20], which we used in this comparison, do not include any fitting parameters. Therefore, well below the instability threshold in Δ, the hydrostatic solution yields a quantitatively accurate leading-order description of the system.

At aspect ratios *well above* the instability threshold we always observed several clusters nucleating at the wall opposite to the driving wall. The cluster dynamics [Fig. 2(a)–2(c)] proceeds as gas-mediated competition and coarsening (sometimes as direct mergers) of clusters, in accord with hydrodynamic simulations [16]. As time increases, the number of clusters goes down, and only one dense cluster, fluctuating around its average position in one of the two corners, opposite to the thermal wall, finally survives. Figure 2(c) shows a snapshot of the final state for $\Delta = 3$. For comparison, Fig. 2(d) shows a density map of the final steady state obtained by Livne in a *hydrodynamic* simulation for the same hydrodynamic parameters. The center-of-mass position Y_c of the steady state agrees well with the average-in-time center-of-mass position, measured in the EMD simulations, as shown by the circle in Fig. 6. This indicates that, well above the instability threshold, the hydrostatic theory describes the steady states of the system well. We can also refer the reader to the recent EMD simulation results for *very* large aspect ratios [17]. As no appreciable fluctuations around a broken-symmetry steady state were reported, one can safely assume that the broken-symmetry steady states observed in Ref. [17] should be also describable by the hydrostatic theory.

The system behavior changes dramatically, however, as the aspect ratio Δ approaches Δ_c. We found that, in a wide region of Δ around Δ_c, the final state of the system exhibits large-amplitude irregular oscillations as dense clusters at the wall opposite to the driving wall nucleate, move in the lateral
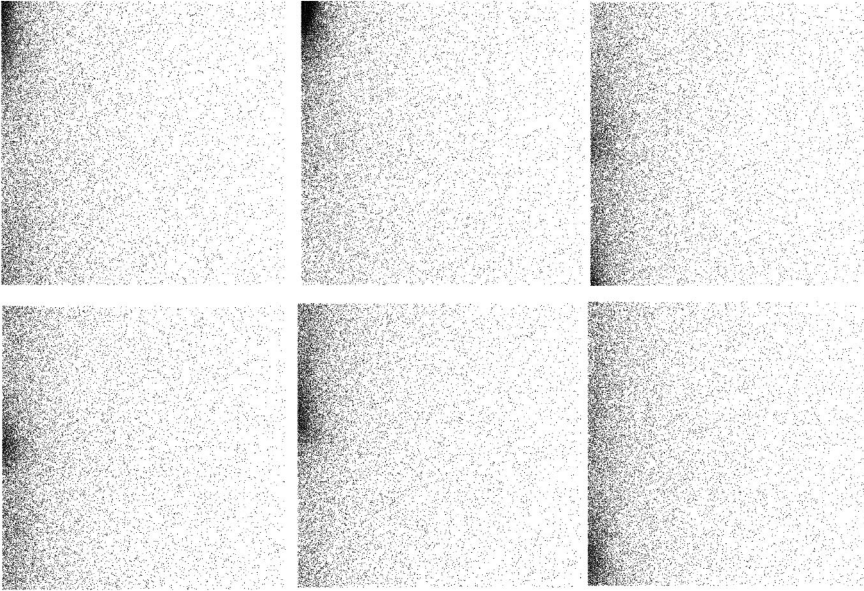
FIG. 3. Irregular lateral cluster dynamics for $\Delta = 1$ as observed in an EMD simulation with $N = 2 \times 10^4$ particles for $\eta = 11\,050$ and $f = 0.025$. The time progresses from left to right, starting from the upper row. The hot wall is on the right.

direction, dissolve, and reappear. Figure 3 shows a typical sequence of snapshots from an EMD simulation for $\Delta = 1$.

Figure 4 shows the time history of the center-of-mass coordinate Y_c for six different values of Δ. One can see that, in a wide region of intermediate Δ, the center-of-mass coordinate $Y_c(t)$ shows large-amplitude irregular oscillations. Noticeable are multiple zero crossings of $Y_c(t)$ at aspect ratios above the hydrodynamic bifurcation point $\Delta_c \simeq 0.514$ [Figs. 4(c)–4(e)]. Smaller but still significant irregular oscillations
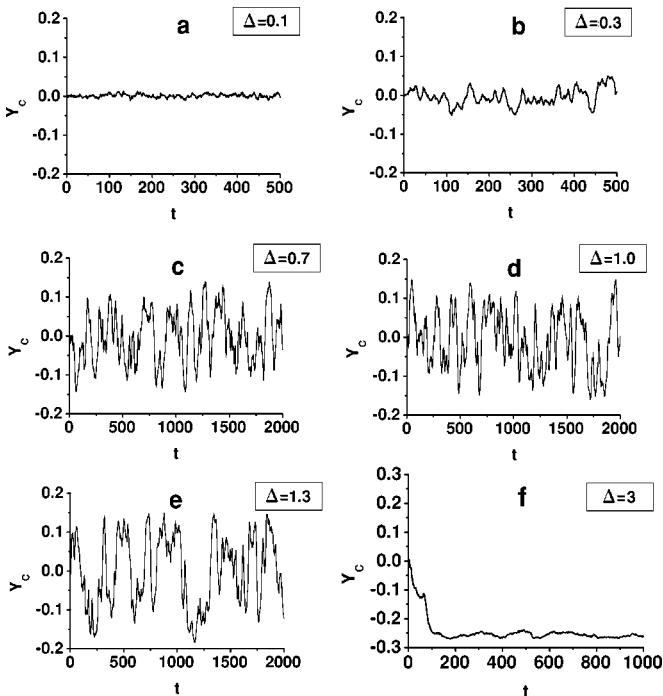

FIG. 4. Y_c vs time for $\eta = 11\,050$ and $f = 0.025$ and different values of the aspect ratio Δ, as observed in EMD simulations with $N = 2 \times 10^4$ particles. Time here is proportional to the number of particle collisions; $t = 500$ corresponds to 505 036 scaled time units.

are also observed below Δ_c, as if the system persistently tends to break the lateral symmetry there. The hydrostatic picture is recovered when one moves farther away, in any direction, from the region of $\Delta \sim \Delta_c$. Indeed, Fig. 4(e) shows that zero crossings of $Y_c(t)$ occur less often for $\Delta = 1.3$ than for $\Delta = 0.7$ or 1. At still larger Δ [Fig. 4(f)] no zero crossings are observed for any reasonable simulation time, and Y_c fluctuates around a constant value that is very close to that predicted by the hydrostatic theory (and shown by the circle in Fig. 6).

To better characterize the fluctuation-dominated region, we computed the probability distribution function $P(|Y_c|)$ of different values of $|Y_c|$ in a statistical steady state, that is, after transients die out. The stationarity of the remaining data was tested by dividing the respective time interval into three subintervals and checking that the differences in $P(|Y_c|)$ for the subintervals are small and not systematic. The probability distribution $P(|Y_c|)$ is shown, at different Δ, in Fig. 5. At $\Delta \ll \Delta_c$ the maximum of $P(|Y_c|)$ is at $|Y_c| = 0$, and it is relatively narrow. Correspondingly, there is no symmetry breaking there, the fluctuations are relatively small, and the hydrostatic theory yields an accurate leading-order description. At $\Delta \gg \Delta_c$, the maximum of $P(|Y_c|)$ is at a nonzero $|Y_c|$. This is a clear manifestation of symmetry breaking: a dense cluster develops in one of the corners away from the driving wall. The probability distribution $P(|Y_c|)$ is also quite narrow here, the fluctuations are relatively small, and there is a good agreement between the hydrostatic theory and EMD simulations. On the contrary, in a wide region of Δ around Δ_c, the probability distribution $P(|Y_c|)$ is very broad, and the hydrostatic theory breaks down. By following the position of the maximum of $P(|Y_c|)$ at different Δ (see Fig. 6), one can see that the symmetry-breaking transition occurs somewhere in the region of $0.3 < \Delta < 1.0$. Because of the extreme flatness and broadness of the probability distribution $P(|Y_c|)$ in this region, a more accurate estimate of the position of the maximum of $P(|Y_c|)$ requires a much better sta-
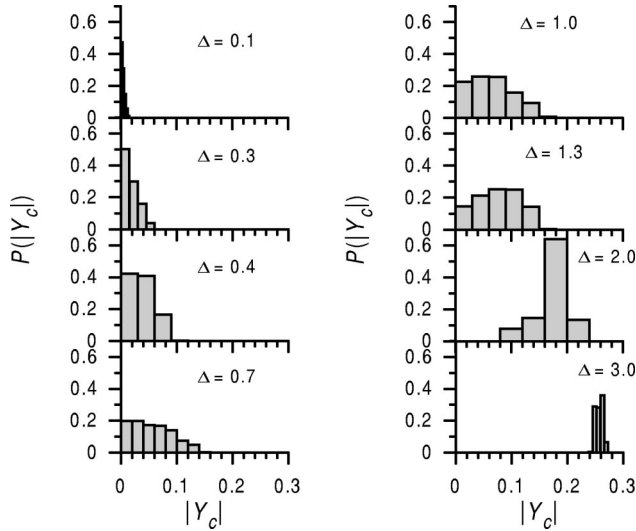
FIG. 5. The probability distribution function $P(|Y_c|)$ of the fluctuating final state of the system for $\eta = 11\,050$ and $f = 0.025$ and different values of the aspect ratio Δ, as observed in EMD simulations with $N = 2 \times 10^4$ particles. In order to show all the graphs on the same scale, the probabilities (rather than the probability densities) for each bin are shown.

FIG. 7. Y_c vs time for $\eta = 11\,050$, $f = 0.025$, and $\Delta = 0.1$ for $N = 5000$ (a), 10 000 (b), 15 000, (c), and 20 000 (d), as observed in EMD simulations. Time units are the same as in Fig. 4.

tistics (that is, a much longer simulation time) than we could afford in this series of simulations [26].

Noticeable in Fig. 6 is a systematic discrepancy, within the wide fluctuation-dominated region, between the positions of the maxima of $P(|Y_c|)$ and the hydrostatic bifurcation curve computed in Sec. III. We even cannot exclude a change in the character of bifurcation caused by the fluctuations (apparently without shifting the bifurcation point). Indeed, the maxima of $P(|Y_c|)$ at $\Delta = 1.0$, 1.3, and 2.0 appear
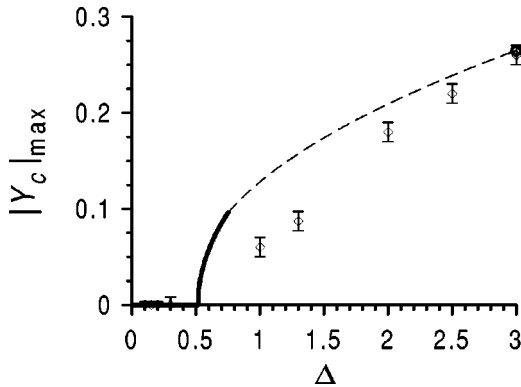

FIG. 6. The effective bifurcation diagram of the system for $\eta = 11\,050$ and $f = 0.025$, observed in EMD simulations with $N = 2 \times 10^4$ particles. Diamonds show, for each Δ, the positions of the maxima of the probability distribution function $P(|Y_c|)$. Above the transition, the error bars show the errors in the estimation of the position of the maximum of $P(|Y_c|)$. Below the transition the error bars show the errors in the estimation of $\langle Y_c \rangle$: the time average of Y_c. The solid line is the bifurcation curve (11) close to threshold. The empty circle at $\Delta = 3$ shows the result of the hydrodynamic simulation by Livne. The dashed line is an interpolation between the solid line and the empty circle.
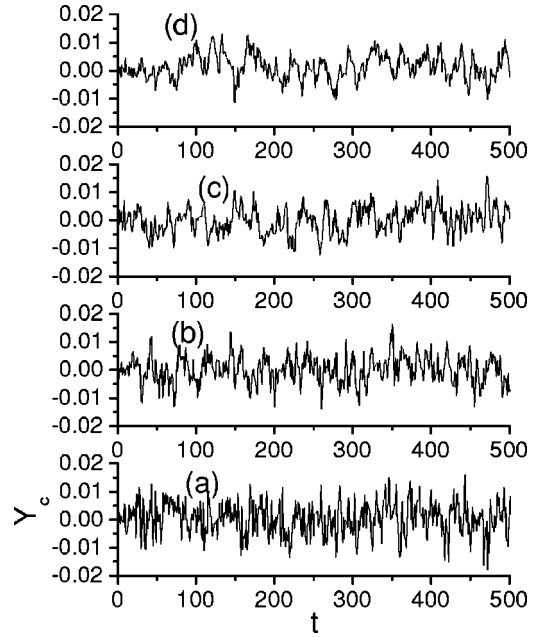
to lie on a straight line passing through the theoretical transition point $\Delta_c \simeq 0.5$. As Δ increases further, the discrepancy between the positions of the maxima of $P(|Y_c|)$ and the theoretical bifurcation curve goes down [25]. Importantly, the fluctuation-dominated region $0.3 < \Delta < 1.0$ does include the hydrostatic transition point $\Delta_c \simeq 0.5$.

We should stress that the failure of hydrostatics is observed at *intermediate* values of the aspect ratio Δ, when the hydrodynamic parameters η and f and the number of particles N are fixed. In view of Eq. (12), while increasing Δ, one increases the inelasticity of particle collisions $1 - r$. That the hydrostatic theory fails at intermediate values of the inelasticity, and improves at small enough or large enough inelasticities, excludes the inelasticity itself as the reason for the failure.

C. Simulations with different N

We did a series of simulations with different number of particles N in order to verify the hydrostatic scaling and investigate the N dependence of the (relatively weak) fluctuations well below and well above Δ_c. These additional simulations were done for $\Delta = 0.1$ and three values of N, 5×10^3, 10^4, and 1.5×10^4, and for $\Delta = 3.0$ and $N = 4 \times 10^4$.

When varying N at fixed Δ, we kept the hydrodynamic parameters $\eta = 11\,050$ and $f = 0.025$ constant. Therefore, if the hydrostatic equations provide a correct leading-order theory of the steady states far below and far above Δ_c, the time-averaged steady-state values of Y_c should become N independent for large enough N. Figure 7 shows Y_c versus time for $\Delta = 0.1$ at the four different values of N. One can see that, in all these cases, the average value of Y_c is close to zero as expected, while fluctuations are relatively small. Figure 8 shows the dynamics of $Y_c(t)$ for $\Delta = 3$ and two differ-
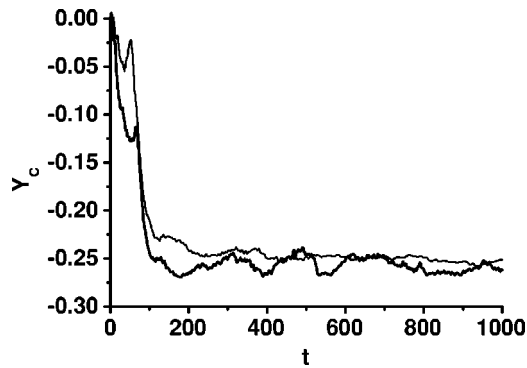
FIG. 8. Y_c vs time for $\eta = 11\,050$, $f = 0.025$, and $\Delta = 3$ for two different values of N, as observed in EMD simulations. The thick line corresponds to $N = 2 \times 10^4$ and the thin line corresponds to $N = 4 \times 10^4$. Time units are the same as in Fig. 4.

ent values of N: 2×10^4 and 4×10^4. Here the symmetry breaking is evident as a dense cluster develops in a corner. With a moderate accuracy determined by the relatively high level of fluctuations of Y_c, the average values of Y_c at late times are close to each other. Therefore, well below and well above Δ_c the hydrostatic scaling is obeyed.

Simulations with fixed scaled parameters η, f, and Δ but different N can also help in identifying the mechanism of breakdown of the hydrostatic theory at aspect ratios around Δ_c. Indeed, it is natural to interpret the giant oscillations, shown in Figs. 4(c)–4(e) in terms of a strong coupling between the two bifurcated states predicted by the hydrostatic theory. One possible scenario of this coupling (which we call scenario I) relies on the discrete-particle noise, unaccounted for by granular hydrodynamics. Below Δ_c, the discrete-particle noise is expected to cause fluctuations, that is, to broaden the distribution of Y_c as indeed observed in Fig. 5. If scenario I is correct, the standard deviation σ of $Y_c(t)$ from its average value should vanish as N goes to infinity, at fixed hydrodynamic parameters η, f, and Δ.

Another possibility (scenario II) is that the fluctuations persist in the limit of $N \to \infty$. If this is the case, the dominating mechanism of fluctuations has a purely hydrodynamic nature and should be explainable by a *full* hydrodynamic analysis (as opposed to our hydrostatic analysis, and to the simplified hydrodynamic simulations that used a model Stokes friction instead of the full viscosity). Here the coupling between the two symmetry-broken states may be due to either an unstable hydrodynamic mode (scenario IIa) or a weakly damped mode (scenario IIb). In scenario IIb, σ should vanish, as $N \to \infty$, if one waits for a sufficiently long time. Therefore, to distinguish between the two subscenarios, one should, in addition to the limit of $N \to \infty$, take the limit of $t \to \infty$.

Obviously, one is unable to take any of these two limits in actual EMD simulations, where the maximum achievable values of N and t are limited by the available computer resources. So what was observed in our EMD simulations with different N? Figures 7 and 9 show what happens well below Δ_c, when N increases from 5000 to 20 000. One can see from Fig. 7 that, as N grows, the high-frequency components of the fluctuations do decrease, but the low-frequency com-
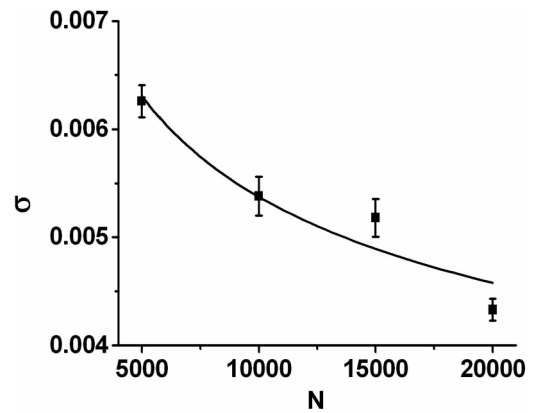

FIG. 9. Shown is σ, the standard deviation of Y_c from its (almost zero) average value, vs the number of particles N for $\eta = 11\,050$, $f = 0.025$, and $\Delta = 0.1$. The symbols show the simulation results. The curve shows, as a reference, the power-law dependence $\sigma = BN^{-\beta}$ with exponent $\beta = 0.23$, see the text.

ponent does not show any pronounced decrease. Overall, the fluctuation spectrum moves towards the lower frequencies. As the result, a good resolution of the low-frequency part of the power spectrum requires longer and longer simulations (which rapidly become prohibitively long). This introduces an additional, nontrivial constraint on simulations with a large number of particles. A similar situation occurs well above Δ_c. Figure 8 does indicate that σ goes down as N goes up from 20 000 to 40 000. However, one also observes that, as N grows, the role of the low-frequency components of the fluctuations increases.

Hydrodynamics provides a hint for the mechanism of the "redshift" of the power spectrum with an increase of N. There are four hydrodynamic modes in the system: two acoustic modes, the entropy mode, and the shear mode. The frequencies of the acoustic modes are the highest, as they are determined by the "ideal" (nondissipative) terms in the hydrodynamic equations, and they scale like the inverse system size. The frequencies of the entropy and shear modes are much lower as they are determined by the transport coefficients, the heat conduction, viscosity, and inelastic loss rate, and they scale like the inverse *square* of the system size. In the units of $d = m = T_0 = 1$, and at fixed hydrodynamic parameters η, f, and Δ, a larger N implies a larger system, see Eqs. (13). Correspondingly, as N increases, the characteristic frequencies of the entropy/shear modes go down much faster than those of the acoustic modes. Therefore, it seems likely that one of these modes is responsible for the low-frequency components of the fluctuations. A related issue is that, in contrast to the hydrostatic problem (1), the full time-dependent hydrodynamic problem has an additional scaled parameter d/L_x. This parameter describes the role of the dissipative terms compared to the ideal terms in the hydrodynamic equations. As it is clear from Eq. (13), when increasing N at constant η and f, one reduces this additional parameter. Therefore, as N increases, the low-frequency shear/entropy modes should become more and more persistent. As these modes are not necessarily broadband, σ might

cease to provide a good characterization of the system at large N.

Still, if one continues following σ as N increases, one observes (see Fig. 9) that σ decreases much more slowly than the classic dependence $N^{-1/2}$ characteristic of equilibrium systems. If one attempts to interpret the decrease of σ with an increase of N in terms of an empirical power law, one obtains an exponent -0.23, instead of the classical value of $-1/2$ for equilibrium systems. Importantly, we did reproduce the classic $N^{-1/2}$ scaling of σ in a control series of simulations with the same f and Δ, but with $\eta = 0$ (elastic collisions). Moreover, a good quantitative agreement was obtained with a theoretical result for σ that directly follows from the classic expression for the density correlation function in equilibrium [27]. We also found that, for the same total number of particles N, the fluctuation levels in the elastic case are significantly lower than in the inelastic case. That is, well below Δ_c, the fluctuations, though much smaller than those observed for $\Delta \sim \Delta_c$, are still large compared to the elastic case.

Overall, our simulations with different N strongly indicate that the hydrostatic equations provide a correct leading-order theory of this system well below and well above Δ_c. On the other hand, the simulations proved to be insufficient for determining the mechanism of giant fluctuations that we observed in this system at $\Delta \sim \Delta_c$. We cannot even be sure at this point whether the fluctuations (or, more precisely, their low-frequency components) persist or not as $N \to \infty$.

V. SUMMARY AND DISCUSSION

The main results of this work can be summarized in the following way. Granular hydrostatics, in combination with simplified hydrodynamic simulations, correctly predict the phase separation instability in this prototypical driven granular system. Well above and well below the critical value of the aspect ratio Δ_c, the hydrostatic theory describes the steady state of the system well. However, in a wide region of aspect ratios around Δ_c the system is dominated by fluctuations and the hydrostatic theory fails. The fluctuation levels are anomalously high even relatively far from the hydrostatic bifurcation point, and they certainly do not exhibit the classic $N^{-1/2}$ scaling with the number of particles N.

Though we are unable to pinpoint the mechanism of excitation of the giant fluctuations, we can suggest two different scenarios for their origin. In scenario I the fluctuations are driven by discrete-particle noise. Indeed, it is well known that discrete-particle noise can drive relatively large fluctuations in the vicinity of thresholds of hydrodynamic instabilities [12] and nonequilibrium phase transitions [28]. Unfortunately, our simulations with different N, but fixed η, f, and Δ, have been insufficient to prove or disprove this scenario.

A difficulty with scenario I is that the fluctuations are so big in so wide a region of aspect ratios. No anomaly of this type has been observed in any other symmetry-breaking instability of granular flow, even with much smaller numbers of particles. As an example, let us consider for a moment the same system, but introduce gravity in the x direction. Now

the granular gas is heated from below, and the system exhibits *another* symmetry-breaking instability: thermal convection, similar to the Rayleigh-Bénard convection of classical fluids. The transition to convection occurs via a supercritical bifurcation [29–31]. Though EMD simulations of thermal granular convection [29] involved only $N = 2300$ particles (which is much less than $N = 2 \times 10^4$ used in the present work), a *sharp* supercritical bifurcation was observed, in agreement with a hydrodynamic analysis [30,31]. By comparison, the giant fluctuations, observed in a wide region of Δ in the present work, are an anomaly, as one needs some (hydrodynamic?) mechanism of strong *amplification* of the discrete-particle noise.

If scenario I proves to be correct, the corresponding theory can be developed in the framework of fluctuating hydrodynamics [27], generalized to granular gases in the limit of nearly elastic collisions. Fluctuating hydrodynamics is a Langevin-type theory that takes into account the discrete character of particles by adding δ-correlated noise terms in the momentum and energy equations [27]. Fluctuating hydrodynamics is by now well established for classical fluids in 3D, including nonequilibrium states [12,32]. We should mention here that the 2D case has an additional difficulty. The coupling of fluctuations here is anomalously strong, even in the elastic case: the transport coefficients diverge in the thermodynamic limit, except for a sufficiently dilute gas [33]. Therefore, one can hope to generalize the fluctuating hydrodynamics to the 2D gas of inelastic hard spheres in the dilute limit [34]. Close to the phase separation threshold, the dilute limit holds with a reasonable accuracy. It would be interesting to investigate the phase separation problem in 3D, where important differences in the fluctuation behavior may occur.

Alternatively, in scenario II the low-frequency component of the giant fluctuations has a purely hydrodynamic origin and is driven either by a presently unknown hydrodynamic instability (scenario IIa) or by a long-lived transient mode (scenario IIb). Effects of these types are obviously missed by a *hydrostatic* analysis. They may have also been missed by the time-dependent hydrodynamic simulation [23] that employed a model Stokes friction, rather than the hard-sphere viscosity, to accelerate the convergence to a steady state. If scenario II is correct, the low-frequency component of the fluctuations should be observable in hydrodynamic simulations with the true hard-sphere viscosity. These simulations, therefore, should be an important next step in the analysis of this fascinating problem.

[1] L.P. Kadanoff, Rev. Mod. Phys. **71**, 435 (1999).

[2] *Granular Gases*, edited by T. Pöschel and S. Luding (Springer, Berlin, 2001); *Granular Gas Dynamics*, edited by T. Pöschel and N. Brilliantov (Springer, Berlin, 2003).

[3] P.K. Haff, J. Fluid Mech. **134**, 401 (1983); J.T. Jenkins and M.W. Richman, *ibid.* **192**, 313 (1988); C.S. Campbell, Annu. Rev. Fluid Mech. **22**, 57 (1990), and references therein.

[4] I. Goldhirsch and G. Zanetti, Phys. Rev. Lett. **70**, 1619 (1993); A. Kudrolli, M. Wolpert, and J.P. Gollub, *ibid.* **78**, 1383 (1997); J.S. Olafsen and J.S. Urbach, *ibid.* **81**, 4369 (1998); D. van der Meer, *et al.*, *ibid.* **88**, 174302 (2002); K. van der Weele *et al.*, Europhys. Lett. **53**, 328 (2001); B. Meerson, T. Pöschel, and Y. Bromberg, Phys. Rev. Lett. **91**, 024301 (2003).

[5] H.M. Jaeger, S.R. Nagel, and R.P. Behringer, Rev. Mod. Phys. **68**, 1259 (1996); R.D. Wildman, J.M. Huntley, and D.J. Parker, Phys. Rev. Lett. **86**, 3304 (2001); Y. Forterre and O. Pouliquen, *ibid.* **86**, 5886 (2001).

[6] P.B. Umbanhowar, F. Melo, and H.L. Swinney, Nature (London) **382**, 793 (1996).

[7] E.C. Rericha *et al.*, Phys. Rev. Lett. **88**, 014302 (2002).

[8] T. Pöschel, N. Brilliantov, and T. Schwager, Int. J. Mod. Phys. C **13**, 1263 (2003).

[9] S.E. Esipov and T. Pöschel, J. Stat. Phys. **86**, 1385 (1997).

[10] E.L. Grossman, T. Zhou, and E. Ben-Naim, Phys. Rev. E **55**, 4200 (1997).

[11] M.L. Tan and I. Goldhirsch, Phys. Rev. Lett. **81**, 3022 (1998); J.J. Brey and D. Cubero, Phys. Rev. E **57**, 2019 (1998).

[12] P.C. Hohenberg and J.B. Swift, Phys. Rev. A **46**, 4773 (1992), and references therein; G. Quentin and I. Rehberg, Phys. Rev. Lett. **74**, 1578 (1995); M. Wu, G. Ahlers, and D.S. Cannell, *ibid.* **75**, 1743 (1995).

[13] E. Livne, B. Meerson, and P.V. Sasorov, e-print cond-mat/008301; Phys. Rev. E **65**, 021302 (2002).

[14] J.J. Brey, M.J. Ruiz-Montero, F. Moreno, and R. García-Rojo, Phys. Rev. E **65**, 061302 (2002).

[15] E. Khain and B. Meerson, Phys. Rev. E **66**, 021306 (2002).

[16] E. Livne, B. Meerson, and P.V. Sasorov, Phys. Rev. E **66**, 050301(R) (2002).

[17] M. Argentina, M.G. Clerc, and R. Soto, Phys. Rev. Lett. **89**, 044301 (2002).

[18] T.P.C. van Noije and M.H. Ernst, in *Granular Gases* (Ref. [2]), p. 3; J.J. Brey and D. Cubero, *ibid.*, p. 59; I. Goldhirsch, *ibid.*, p. 79.

[19] J.J. Brey, J.W. Dufty, C.S. Kim, and A. Santos, Phys. Rev. E **58**, 4638 (1998).

[20] J.T. Jenkins and M.W. Richman, Phys. Fluids **28**, 3485 (1985).

[21] E. Khain, B. Meerson, and P.V. Sasorov (unpublished).

[22] G. Iooss and D.D. Joseph, *Elementary Stability and Bifurcation Theory* (Springer, New York, 1980), p. 88.

[23] The hydrodynamic simulation was done with the constitutive relations by Grossman *et al.*, [10], more accurate at large densities. In addition, the gas-kinetic viscosity in the momentum equation was replaced in this simulation, as well as in the simulations [13,16], by a moderately large Stokes friction. Obviously, the Stokes friction does not affect hydrostatic steady states. However, it cannot provide a faithful description of the *shear modes* in a gas of hard spheres.

[24] B.J. Alder and T.E. Wainwright, J. Chem. Phys. **27**, 1208 (1957); D.C. Rapaport, J. Comput. Phys. **34**, 184 (1980); M. Marìn, D. Risso, and P. Cordero, *ibid.* **109**, 306 (1993).

[25] Notice that, for large aspect ratios, hydrodynamic simulations are not expected to give a high accuracy for an entirely different reason. The density of the symmetry-broken cluster here approaches the close-packing density, while the accuracy of the interpolating constitutive relations [10] is not very high.

[26] A single simulation such as those shown in Figs. 4(c), 4(d), or 4(e) requires about 350 h of the CPU time of a Pentium P4 at 1.4 GHz.

[27] E.M. Lifshitz and L.P. Pitaevskii, *Statistical Mechanics* (Pergamon Press, Oxford, 1980), Pt. 2, Sec. 88.

[28] H. Haken, *Synergetics* (Springer, Berlin, 1983); J. García-Ojalvo and J. Sancho, *Noise in Spatially Extended Systems* (Springer, New York, 1999).

[29] R. Ramìrez, D. Risso, and P. Cordero, Phys. Rev. Lett. **85**, 1230 (2000).

[30] X. He, B. Meerson, and G. Doolen, Phys. Rev. E **65**, 030301(R) (2002).

[31] E. Khain and B. Meerson, Phys. Rev. E **67**, 021306 (2003).

[32] M. Malek Mansour *et al.*, Phys. Rev. Lett. **58**, 874 (1987); A.L. Garcia *et al.*, Phys. Rev. A **36**, 4348 (1987).

[33] B.J. Alder and T.E. Wainwright, Phys. Rev. A **1**, 18 (1970); P.M.V. Résibois and M. de Leener, *Classical Kinetic Theory of Fluids* (Wiley, New York, 1977).

[34] Unfortunately, recent attempts to employ fluctuating hydrodynamics in the context of a freely evolving [35] and randomly driven [36] dilute *granular* gas are incomplete, as they do not account for an important additional Langevin term in the energy equation, arising because of the discreteness of the collisional energy losses.

[35] T.P.C. van Noije, M.H. Ernst, and R. Brito, Phys. Rev. E **57**, R4891 (1998).

[36] T.P.C. van Noije *et al.*, Phys. Rev. E **59**, 4326 (1999).

[37] See http://bioinf.charite.de/kies/giantfluctuations/